Investigation on residual stresses in milling of Ti-6Al-4V for both rake and flank application of different MWF strategies

Anshab Kummamkandath, Arnaud Duchosal, Antoine Morandeau, René Leroy

Available online at www.sciencedirect.com

ScienceDirect

Procedia CIRP 00 (2019) 000–000

www.elsevier.com/locate/procedia

5th CIRP CSI 2020

Investigation on residual stresses in milling of Ti-6Al-4V for both rake and flank application of different MWF strategies

Anshab Kummamkandath[a,b,*], Arnaud Duchosal[a], Antoine Morandeau[b,c], René Leroy[a]

[a]*Univ. Tours, Univ. Orléans, INSA CVL, LaMé, F-37200 Tours, France*
[b]*Sandvik Coromant, 4 Avenue Buffon, 45100 Orleans, France*
[c]*Advanced Assisted Manufacturing Solutions (AAMS), Bâtiment CEROC, Rue Henri Garih, 37230 Fondettes, France*

* Corresponding author. Tel.: +33-768653144. *E-mail address:* anshab.ka@sandvik.com

Abstract

This study investigates the effects of both rake and flank applications of different Metal Working Fluid (MWF) strategies on residual stresses in the machining of Ti-6Al-4V alloy. Cryogenic (Liquid CO_2), Minimum Quantity Lubrication (MQL) and emulsion strategies were studied with modified CoroMill600 milling cutter via internal channels delivering media to insert rake face and flank face. The cutting force, minimum chip thickness and chip morphology were analyzed to understand more about this novel approach of rake and flank delivery of different MWFs in milling. The results reveal the formation of compressive residual stresses until 55-60µm beneath the machined surface irrespective of the type of MWF strategies. The highest value of compressive residual stress was observed at the machined surface of liquid CO_2. The magnitude of the traced compressive residual stress profile shows a trend of positive slope gradient beneath the surface for both parallel and perpendicular to feed directional residual stress components. In contrast, residuals stresses in emulsion and MQL strategies were observed with a different trend in generation of compressive residual stress components, where the parallel to feed directional component shows an inflection point with a an initial negative slope gradient followed by a positive one to beneath the machined surface. An increase in the cutting forces and minimum chip thickness values were also observed for liquid CO_2, due to the high shear resistance of Ti-6Al-4V alloy at machining zone, which was confirmed from the chip morphology analysis. Overall results show that cryogenic CO_2 leads to higher compressive residual stresses at the surface and positive slope gradient beneath the material. The higher cutting forces in Z-axis and minimum chip thickness value in liquid CO_2 are also attribute to the higher compressive stresses in Ti-6Al-4V workpiece at cryogenic CO_2 environment.

Keywords: Cryogenic machining; rake and flank application; residual stress.

1. Introduction

Residual stress is one of the important surface integrity parameters in many industrial applications, mainly for the aerospace application of superalloys; because it has a critical decisive role to define the performances and service lifespan of specific components. Previous investigations have already reported about the impact of thermal and mechanical load effects in residual stress generation while machining of superalloys, particularly for the Ti-6Al-4V alloy and show that mechanical load leads to suppress the tensile residual stress; whereas thermal load promotes it [1]. These studies display the effectiveness of different Metal Working Fluid (MWF) strategies and its considerable impact on the magnitude and direction of the accumulated residual stress in machined Ti-6Al-4V workpieces. An efficient cooling condition can reduce the magnitude of tensile residual stresses as a result of reduction in the thermal load contribution, whereas an increase

in mechanical load leads to more cutting force and compressive residual stress generation [1, 2]. However, some previous reports claim that the type and magnitude of the residual stresses depends on how this mechanical load is applying as well as its magnitude [3]. The residual stress in the machined workpiece surface also get influenced by the relative magnitude of both tensile and compressive loads; where a predominantly compressive load over the material ahead of the cutting tool will induce the tensile residual stress; vice versa, a predominant tensile loading generates compressive residual stress [4].

Nature and application strategies of the MWFs have a key role to describe the effectiveness of thermo-mechanical loads in Ti-6Al-4V machining which defines the machinability of the process. Several studies have already been reported for the excellence of cryogenic cooling over the low thermal conductivity nature and related higher tool wear issues facing in machining Ti-6Al-4V alloys. It also considers as the best alternative solution for critical sustainability issues of conventional emulsion cooling strategies [2-4] in terms of improved surface integrity [3,5] and tool wear progression [4,6]. However, among the surface integrity studies; only a limited number of studies were investigated on the residual stress development under cryogenic machining of Ti-6Al-4V alloy, out of those, the main focus were made on the LN_2 assisted machining strategies [1,7].

A number of researches have come up by showing that optimal flow of cryogens and position of the outlet nozzles close to the cutting edge of the tool have a significant role to define the effectiveness and consistency of the cryogenic machining process. Influences of the liquid CO_2 flow rate on Ti-6Al-4V milling tool life have also been reported in the literature [6]. The cold strength hardening of the Ti-6Al-4V workpiece and related unpredictable results (due to early-stage breakdown of cutting tools) are the main challenges in cryogenic machining under LN_2 [10], later the rake and flank precise turning application of LN_2 was reported with improved machinability [11]. It reduces cold strength hardening and promotes efficient cooling [12] compared to the cryogen rake face or flank face standalone applications and emulsion strategies; via less exposure of the cryogen to the workpiece and more reachability to the machining zone. In general, the consistency of the cryogenic machining of Ti-6Al-4V mainly depends on the position of outlet nozzles towards the cutting edge and optimum flow of the cryogen. This work mainly proposes a novel milling cutter design (TRL7) strategy with more precise application of MWFs to both rake and flank faces of the inserts via internal channels. Therefore, this novel delivery approach was evaluated in terms of generated residual stresses at the surface and subsurface of the machined Ti-6Al-4V alloy. Furthermore, the cutting forces, chip morphology and minimum thickness analysis were conducted for a detailed understanding of residual stresses generation in different MWF strategies; such as liquid CO_2, MQL and emulsion.

2. Experimental setup

The machining experiments presented in this work consist of face milling of Ti-6Al-4V alloy for both rake and flank face application of the different MWF strategies such as liquid CO_2, MQL, and emulsion.

The forged and annealed condition Ti-6Al-4V (α-β) alloy was used as workpiece material and the elemental composition of the material is added in Table 1. All the tests were performed in Hermle C40 CNC center with modified CoroMill600 milling cutter (D_{cap} = 59.9mm, D_c = 51mm) and Figure 1 shows the experimental setup.

Table 1. Elemental composition of Ti-6Al-4V workpiece.

Element	Al	V	Fe	N	C	H	O
Composition (wt.%)	6	4	0.19	<0.01	0.02	0.01	0.18

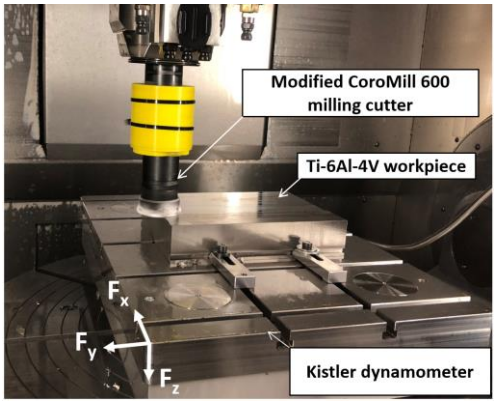

Figure 1. Experiment setup.

Table 2 shows the details of selected MWFs and application details.

Table 2. Description and supply conditions of selected MWF strategies.

MWFs	Description
Liquid CO_2	• E13120 ChilAir system • Supply pressure: 50 bars • CO_2 consumption: 10 kg/ hr.
MQL	• SKF mono-channel MQL generator • MQL oil: VP15009 (Blaser Swisslube) • Based on synthetic polyol esters • Optimized MQL oil for Ti machining • Outlet pressure: 2 bars; Flow rate: 73 ml/ hr
Emulsion	• IGOL USINOV 2475 • Supply pressure: 50 bars. • Additional external jets of emulsion focused to machining zone

The milling cutter was modified by adding internal channels to rake and flank face delivery of the MWFs with an outlet channel diameter of 0.8mm to each face. The tool internal channel modification and outlet channel diameter were selected suitable for all the selected MWF conditions; based on Sandvik Coromant internal references. The tool outlet channel position and distance from the cutting edge are show in Figure 2 in the PR-PP-PF reference frame based on NF-E-66-502 standards. Two PVD coated inserts (600-1252E-ML 1030) were used with an arc of engagement of 180° to the milling cutter. All the

cutting conditions, cutting tool, and inserts were selected based on Sandvik Coromant recommendations.

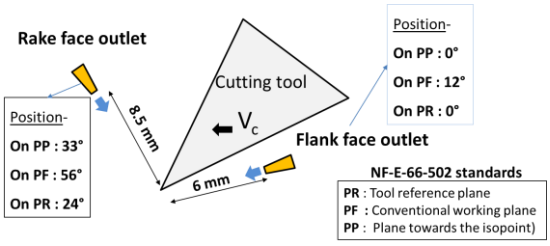

Figure 2. The outlet nozzle position in PP-PR-PF reference plan [NF-E-66-502 standards]

3. Experimental procedure

The experiments were conducted by two phases.

(i). Analyze the residual stress at surface and beneath the surface for machined Ti-6Al-4V for a cutting condition of cutting speed V_c = 90m/min; feed per tooth f_z = 0.17mm/tooth, depth of cut a_p = 2mm; width of cut a_e = 15mm. furthermore, the chip morphology and minimum chip thickness analysis for the same cutting condition.

(ii). Cutting force analysis based on Design of Experiment (DoE) as a function of feed and speed (as per Table 3).

Table 3. shows the corresponding DoE followed for the cutting force analysis.

Ex. no	V_c (m/min)	f_z (mm/tooth)
1	50	0.05
2	100	0.05
3	50	0.15
4	100	0.15
5	50	0.1
6	100	0.1
7	75	0.05
8	75	0.15
9	75	0.1
10	75	0.1
11	75	0.1

Accumulated residual stresses were measured by X-Ray Diffraction (XRD) analysis; beneath the machined Ti-6Al-4V workpiece surface by Bruker D8 Discover equipment. The XRD analysis was conducted initially at the machined surface and then in each 15µm depth beneath the surface until 75µm of total depth for each MWF machined samples Based on references, Cu tube was selected as X-ray source (wavelength λ: 0.1540 nm) with a collimator diameter of 2 mm. The psi (ψ) method was used with an inclination of +/-59° with 9 number of tilts. The diffraction peak for the Millar indices {213} was traced with respect to corresponding Bragg angle 2θ of 141.7°. LectroPol-5 electropolishing machine was used for the precise material removal without inducing any extra residual stresses on the machined surfaces.

Kistler 92553B23 dynamometer was used for the cutting force analysis (see Figure 1), and the Design of Experiment (DoE) window was followed as a function of varying cutting speed and feed (as per Table 3). The face centered central composite design with 3 central point repetition were selected. Based on DoE, 11 tests each with 15 mm machining pass was performed and the details of the selected forces acquisition system are: resolution = 2.5mN, gain = 0.01 pC and range -30kN to 30kN for F_x and F_y. -10kN to 60kN for F_z).

For chip morphology analysis, five chips were collected with controlled tool wear of V_b less than 0.1mm, which were then mounted, polished and etched to analyses the morphologies. Five chips, each with nine serrations, so total of 45 chip serrations were analyzed for the statistical study. Keyence VHX 5000X digital microscope was used for the chip studies; where 0.3µm is the error range in measurements corresponding to 5000X magnification.

4. Results and discussions

4.1. Residual stresses

The residual stresses of the machined Ti-6Al-4V workpiece at surface and sub-surface were studied along the parallel to the feed direction (σ_{11}) and perpendicular to the feed direction (σ_{22}).

Figure 3 shows the corresponding residual stresses resultant profiles for all the three MWF conditions. The compressive residual stress generation is observed in both σ_{11} and σ_{22} direction, at surface and subsurface of the workpiece irrespective of the MWF strategies. The residual stresses effects are observed until 55-60µm beneath the machined surface for all the MWF conditions and below this region the stresses were stable. Comparatively, σ_{22} (perpendicular to feed direction) stress component exhibits higher magnitude of compressive residual stresses than σ_{11} (parallel to feed direction) and this can be ascribed to more cutting load (mechanical load) influences on σ_{22}.

In addition, the higher compressive residual stresses magnitude in the liquid CO_2 for both σ_{11} and σ_{22} reveals that the cryogenic cooling via both rake and flank delivery strategy generates lower thermal load compared to the other MWFs; and hence higher compressive residual stresses. The MWFs type has influences on the maximum compressive residual stress accumulation position. For liquid CO_2 maximum values are noted at the machined surface in both σ_{11} and σ_{22} while in MQL and emulsion, only σ_{22} stress component has a maximum at the machined surface. In the case of σ_{11}, both MQL and emulsion are recorded the highest compressive residual stress value around 16-18µm beneath the machined surface. Therefore, these results display a similar positive gradient trend on the compressive residual stress slope profiles for all two-directional stress components in liquid CO_2; from the surface to until 55-60 µm beneath the machined surface while the other two MWF strategies follow a different trend in σ_{11} and σ_{22} residual stress profiles. An inflection point was observed in the σ_{11} residual stress profile curves with an initial negative slope gradient followed by a positive one whereas the σ_{22} follows a positive slope gradient in traced compressive residual stress profiles like in liquid CO_2. This trend in residual stress components under liquid CO_2 strategy leads to less stress variation in depth which may further prevent the underneath

surface fatigue crack initiation, compared to emulsion and MQL conditions.

Concerning the magnitude of generated residual stress, only at the machined surface is observed with notable influences of coolant nature, underneath the machined surface the compressive residual stresses values are overlapping in all the three MWF strategies.

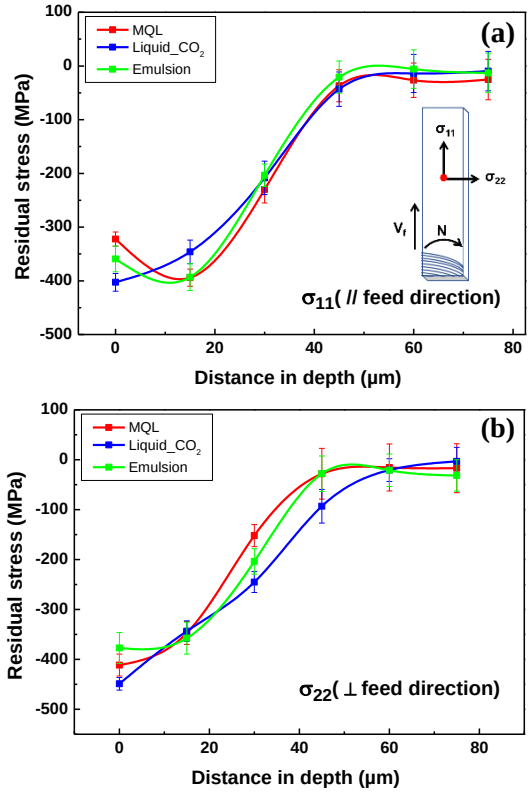

Figure 3. Residual stress profile (a) parallel to feed direction (b) perpendicular to feed direction.

To understand more about the observed residual stress profiles further analysis was performed on the cutting force, minimum chip thickness, and the chip morphology.

4.2. Cutting forces

Cutting forces were measured based on a full factorial Design of Experiment matrix (DoE) with varying cutting speed and feed (as per Table 3). Three orthogonal force components F_x, F_y, and F_z were analyzed from the fixed reference plane of the Kistler table as per Figure 1. Cutting force measurements are done in the middle of cutting load cycle corresponding to the analyzed residual stress points and cutting force component F_c was calculated as a resultant of both F_x and F_y orthogonal force components. The observed contours of the F_c and F_z are presented in Figure 4 and 5 as a function of cutting speed (V_c) and feed for all the three MWF strategies.

A similar trend in F_c contours patterns is observed for both MQL and liquid CO_2 machining; with an initial increment (positive slope gradient) of F_c, followed by a decrement (negative slope gradient) with respect to increase in the cutting speed. Emulsion exhibits a reverse trend, a negative slope gradient followed by a positive one; with respect to increase in the cutting speed. The F_z component also shows similar trends, however the variation of cutting forces was very small under selected cutting speed and feed parametric window.

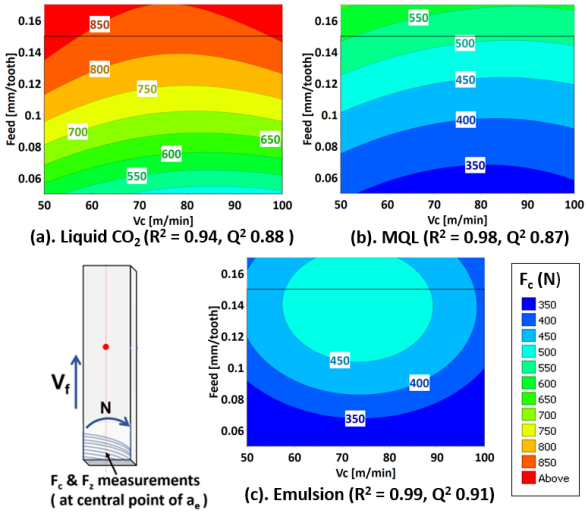

Figure 4. Cutting force component (F_c) contours.

The liquid CO_2 possess higher F_c and F_z compared to both MQL and emulsion that can quantify as an average of 54 % increase in F_c for the liquid CO_2 and there is a 7 % decrease in F_c for MQL compared to the emulsion. In the case of F_z, 13% increase in liquid CO_2 and 7 % decrease in MQL are observed with reference to the emulsion strategy. The increase in the F_c component for liquid CO_2 machining could be due to the increase in shear resistance of the Ti-6Al-4V workpiece at the cryogenic environment. Further studies on h_{min} and chip morphology was performed for more clarification on the same.

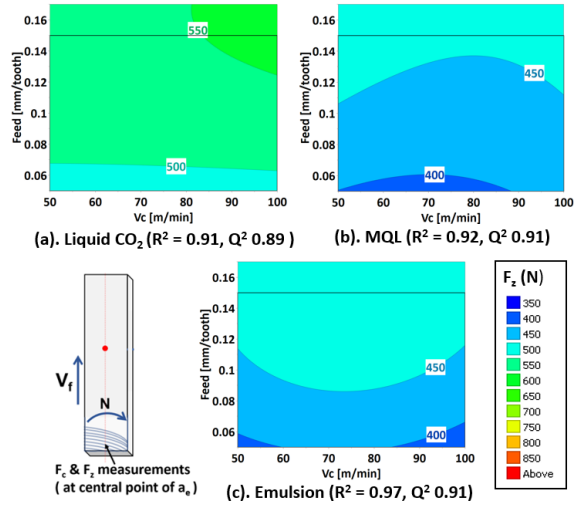

Figure 5. Cutting force component in Z axis (F_z) contours.

In addition, the increase in the F_z component specifies the increase in cutting load normal to the machining surface. The coupled effects of higher compressive cutting load and cryogenic machining environment lead to higher compressive residual stress for liquid CO_2 and the higher compressive residual stresses at the machined surface in both σ_{11} and σ_{22} directional components also attribute to the same hypothesis. Even though the compressive residual stresses in liquid CO_2

varies slightly with respect to the large variation in F_c, clearly shows that the residual stresses generation are closely related to cutting force component in Z (F_z related to compressive mechanical load) than cutting force component F_c. The MQL and emulsion strategies have comparable F_c and F_z resultant response contours.

4.3 Minimum chip thickness (h_{min})

Minimum chip thickness (h_{min}) is a critical decisive factor to define the required specific cutting energy while machining. It describes the required minimum chip thickness when the shearing is predominant in the cutting process [13]. Figure 6 shows the three circumstances in comparison of the uncut chip thickness (h) and minimum chip thickness (h_{min}), for a cutter with r_n edge radius. So, the depth of cut (h) should be at least equal or higher than h_{min} for the effective cutting, otherwise only the phenomena of pressing and elastic deformation (see Figure 6) occurs by consuming higher specific cutting energy. The minimum chip thickness cause the rising of slipping forces and ploughing of the machined surface, which further leads to increase the cutting forces, surface roughness and burr formation [13,14]. Here, the ratio of uncut chip thickness and the edge radius affects the residual stresses [14].

Therefore, the minimum chip thickness defines the point of desired chip thickness and indicates the increase in specific cutting energy values and the cutting mechanism (slipping and shearing). The theoretical specific cutting energy and minimum chip thickness values are calculated by AFNOR E66-520.

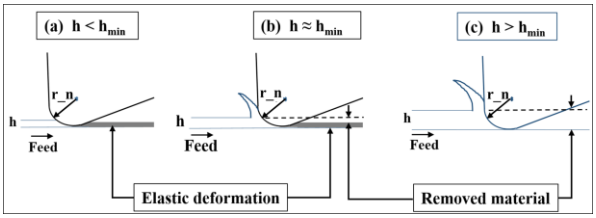

Figure 6. Schematic of the effects of h_{min} in orthogonal cutting [13,15].

According the norm AFNOR E66-520. The theoretical specific cutting energy ($W_{c\ theo}$) is calculated from the experimental specific cutting energy values ($W_{c\ exp}$). The point with 15% deviation between experimental and theoretical curves of W_c attributed as the minimum chip thickness (h_{min}) as per equation 1.

$$\frac{W_{c\,exp} - W_{c\,theo}}{W_{c\,exp}} = 0.15 \qquad (1)$$

Figure 7 shows the corresponding theoretical and calculated specific cutting energy curves versus chip thickness values.

The highest h_{min} value of 0.087mm is observed for liquid CO_2 whereas h_{min} for the MQL is 0.077mm. The analyzed machining window was limited for the emulsion for finding the h_{min} and the corresponding h_{min} value is lesser than 0.048 mm. The difference in the h_{min} indicates material's resistance to the shear deformation during the cutting process; where higher value for liquid CO_2 indicates the higher shear resistance of the Ti-6Al-4V alloy under liquid CO_2 strategy. Previously witnessed higher F_c (cutting force component) and residual stress values are also draw the same conclusion of higher shear resistance of liquid CO_2 environment. The emulsion condition has the lowest h_{min} value and it shows the possible lower uncut chip thickness without crossing the critical specific cutting energy zone in emulsion machining compared to MQL and liquid CO_2.

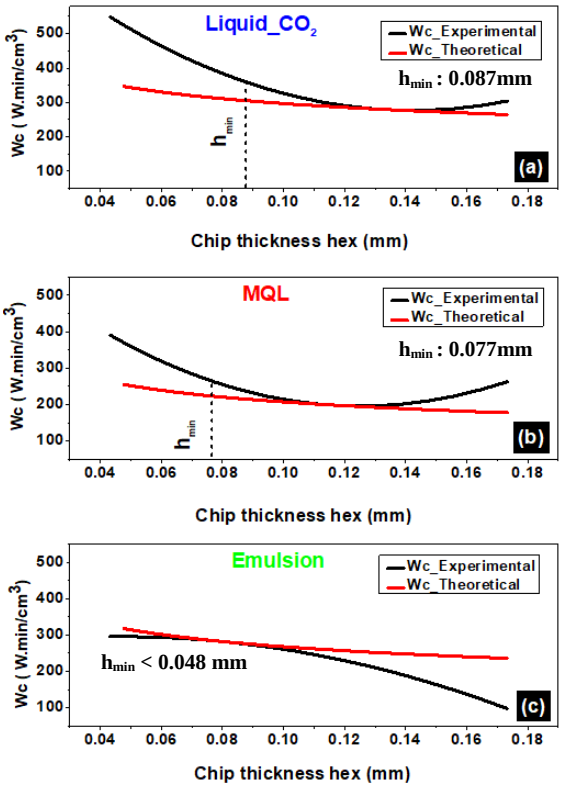

Figure 7. Illustration of the calculating minimum chip thickness value (h_{min}) for (a) Liquid CO_2, (b) MQL and (c) Emulsion strategies.

The chip morphology was also studied in order to understand the material shear behavior for different WMF conditions.

4.3. Chip morphology

Figure 8 shows the chip morphology analysis results under Keyence VHX 5000 digital microscope. Mainly the chip serration frequency was analyzed (as per Figure 9 b) for all the three selected MWF conditions. Lower serration pitch indicates the instability in metal cutting as a result of the adiabatic shear zone due to the low thermal conductivity nature of the Ti-6Al-4V alloy. The serration pitch is inversely proportional to the cutting forces and mentions the higher shear resistance for cutting the material [16].

Figure 9 (a) shows the measured serration pitch for all the three WMF strategies. It is clear that liquid CO_2 condition has higher serration frequency or lower serration pitch ($85.3\ ^{+11}_{-15}$ µm) compared to emulsion ($120.5\ ^{+28}_{-19}$ µm) and MQL ($125.6\ ^{+13}_{-20}$ µm) strategies. Both MQL and emulsion have comparable results and this observation can be linked to the residual stress, cutting force and minimum chip thickness analysis results. The lower temperature at liquid CO_2 via both rake and flank application strategy generates higher shear

resistance in the material and correspondingly increase the cutting forces which further leads to higher accumulation of compressive residual stresses in Ti-6Al-4V surface.

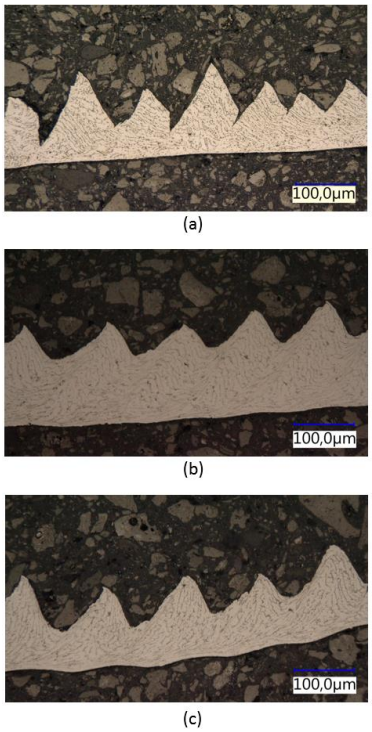

Figure 8. Chip microstructural analysis for (a) Liquid CO_2, (b) MQL and (c) Emulsion strategies.

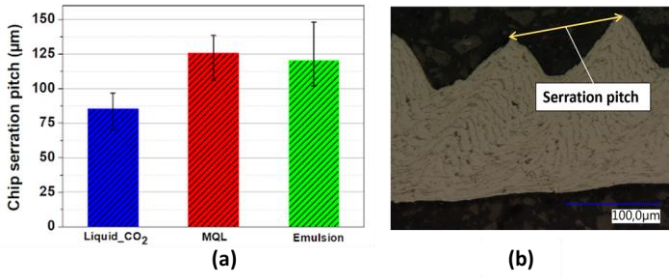

Figure 9. (a) Measured chip serration pitch and (b) measurement strategy.

5. Conclusion

The accrued residual stresses and its effects were investigated in milling of Ti-6Al-4V for the innovative MWFs (metal working fluid) delivery approach; by delivery of MWFs to inserts rake and flank faces. The liquid CO_2, MQL and emulsion strategies were studied with modified milling tool via internal channel flow. The cutting forces, minimum chip thickness, and chip morphology were analyzed for further understanding of the effectiveness of the process. The following conclusions can be drawn from this study:

- The liquid CO_2 machining possess highest magnitude of compressive residual stress generation at the machined surface in both parallel to feed (σ_{11}) and perpendicular to feed (σ_{22}) directions; via coupled effect of higher compressive cutting load and cryogenic cooling environment.
- Both σ_{11} and σ_{22} residual stress components in liquid CO_2 follow a similar trend. Machined surface has the maximum values for compressive residual stress, further continues with a positive slope gradient trend compared to MQL and emulsion.
- Workpiece shear resistance is found to increase for liquid CO_2 strategy at cryogenic machining environment. The increase in the cutting force component (F_c), higher value of calculated minimum chip thickness and lower serration pitch of chip morphology could be linked to the same conclusion. This increase in mechanical cutting load causes to generate higher magnitude compressive residual stresses in Ti-6Al-4V machined surface.

Acknowledgements

The authors would like to express their gratitude to Sandvik Coromant - Västberga (Sweden) and CEROC (France) teams for all the experimental supports; Blaser Swisslube (Switzerland) for providing the MQL oil.

References

[1] Y. Ayed, G. Germain, A. P. Melsio, P. Kowalewski, and D. Locufier, “Impact of supply conditions of liquid nitrogen on tool wear and surface integrity when machining the Ti-6Al-4V titanium alloy,” *Int. J. Adv. Manuf. Technol.*, pp. 93 (1–4), pp.1199–1206, 2019.

[2] I. S. Jawahir *et al.*, “Cryogenic manufacturing processes,” *CIRP Ann. - Manuf. Technol.*, vol. 1557, 2016.

[3] C. R. Liu and M. M. Barash, “The Mechanical State of the Sublayer of a Surface Generated by Chip - Removal Process — Part 1 : Cutting With a Sharp Tool,” *J. Eng. Ind.*, vol. 1976a:1192, p. 1976, 1976.

[4] D. W. Wu and Y. Matsumoto, “The Effect of Hardness on Residual Stresses in Orthogonal Machining of AISI 4340 Steel,” *J. Manuf. Sci. Eng.*, no. 112/3:245-252, p. 4340, 1990.

[5] A. Kummamkandath, A. Duchosal, A. Morandeau, R. Serra, and R. Leroy, “Influence of both rake and flank faces Metal Working Fluid (MWF) strategies on machinability of Ti-6Al-4V alloy,” *MM J.*, no. c, 2019.

[6] M. I. Sadik, S. Isakson, A. Malakizadi, and L. Nyborg, “Influence of coolant flow rate on tool life and wear development in cryogenic and wet milling of Ti-6Al-4V,” *Procedia CIRP*, vol. 46, pp. 91–94, 2016.

[7] B. D. Jerold and M. P. Kumar, “The Influence of Cryogenic Coolants in Machining of Ti – 6Al – 4V,” *J. Manuf. Sci. Eng.*, no. March 2017, 2013.

[8] M. I. Sadik and S. Isakson, “The role of PVD coating and coolant nature in wear development and tool performance in cryogenic and wet milling of Ti-6Al-4V,” *Wear*, vol. 387, pp. 204–210, 2017.

[9] S. Isakson, M. I. Sadik, A. Malakizadi, and P. Krajnik, “ScienceDirect Effect of cryogenic cooling and tool wear on surface integrity in turning of,” *Procedia CIRP*, vol. 00, no. 2212–8271, pp. 3–7, 2018.

[10] M. A. Suhaimi, G. Yang, K. Park, M. J. Hisam, S. Sharif, and D. Kim, “Effect of Cryogenic Machining for Titanium alloy based on Indirect , Internal and External Spray System,” *Procedia Manuf.*, no. 17 (2018) 158–165, pp. 0–7, 2018.

[11] M. J. Bermingham, J. Kirsch, S. Sun, S. Palanisamy, and M. S. Dargusch, “New observations on tool life , cutting forces and chip morphology in cryogenic machining Ti-6Al-4V,” *Int. J. Mach. Tools Manuf.*, vol. 51, pp. 500–511, 2011.

[12] I. Lee, V. Bajpai, S. Moon, J. Byun, Y. Lee, and H. W. Park, “Tool life improvement in cryogenic cooled milling of the preheated Ti – 6Al – 4V,” *Int J AdvManuf Technol*, pp. 665–673, 2015.

[13] F. Ducobu, E. Filippi, and E. Rivière-Lorphèvre, “Chip Formation and Minimum Chip Thickness in Micro-milling,” no. January 2009.

[14] J. C. Outeiro, R. Kandibanda, J. Pina, O. W. Dillon, and I. S. Jawahir, “Size-effects and Surface Integrity in Machining and Their Influence on Product Sustainability,” *Int. J. Sustain. Manuf.*, vol. 2, pp, 2010.

[15] J. Chae, S. S. Park, and T. Freiheit, “Investigation of micro-cutting operations,” *Int. J. Mach. Tools Manuf.*, vol. 46, pp. 313–332, 2006.

[16] S. Joshi, P. Pawar, A. Tewari, and S. S. Joshi, “Infl uence of β phase fraction on deformation of grains in and around shear bands in machining of titanium alloys,” *Mater. Sci. Eng. A*, vol. 618, pp. 71–85, 2014.